

# CHAPTER

---

ENTROPY OPTIMIZED UNSTEADY MHD WILLIAMSON FLUID  
FLOW CONSIDERING VISCOUS DISSIPATION EFFECTS

**Content of this chapter is communicated.**

# Chapter 7

## Entropy optimized unsteady MHD Williamson fluid flow considering viscous dissipation effects

Viscous dissipation is of importance for a variety of applications; for instance, large temperature increases are seen during high-speed polymer manufacturing operations like injection moulding or extrusion. The thin boundary layer surrounding fast aircraft experiences aerodynamic heating, which boosts skin temperature. Due to numerous applications of convective boundary conditions in technology, including thermal energy storage, petroleum processing, material drying etc, we considered convective boundary conditions in this chapter.

### 7.1 Introduction of the Problem

In engineering and industries, non-Newtonian fluids are very important, it compel researchers to investigate the phenomena of mass and heat movement. Shampoos, pulps, Human blood, honey, jelly, sugar, and other non-Newtonian fluids fall into this category. Williamson fluid is a part of pseudo-plastic category. Blood cells, photographic films, food processing, and inkjet printing are some of the applications for pseudo-plastic fluids. We have taken the constitutive equation known as the Williamson model [110] in this study. Consequences of radiation on Williamson fluid discovered by Saravana et al. [109].

Heat is transformed to motion when a liquid is stimulated along a surface in a process known as viscous dissipation. This occurs as a result of a shear power stroke close to the sheet. This phenomena demonstrates an important function in significant industrialised and industrial requests like purification, rock hard, electronic coffee machines, and culinary food. Hsiao [57] scrutinized viscous dissipation effects

on MHD Maxwell fluid with radiation.

Due to its numerous applications in technology, including thermal energy storage, petroleum processing, material drying, etc., the application of convective boundary conditions in heat transfer analysis has distinguished itself among researchers. Convective boundary conditions have recently replaced the usual boundary conditions of constant temperature and constant flux in a number of heat transfer problems. Vaidya et al. [48] explained the chemical reaction on MHD Jeffery nanofluid with convective boundary conditions. Basha et al. [100] scrutinized MHD Carreau fluid with convective boundary conditions. Numerous logical strategies like differential transformation method, least square method, HAM are seen in the writing for tackling the physical and designing issues.

Entropy optimization systems are less competent because they have a higher possibility of becoming irreversible. The first mention of entropy control was made by Bejan [4]. Devi et al. [99] explored entropy generation on MHD fluid flow due to convective heat transfer. Tayebi et al. [129] deliberated the entropy generation on Micropolar fluid flow.

Natural convection flow can be found much of the time in nature. It happens because of positive heat difference, similarly because of mass difference or the merger of these two. Natural convection has broad significance, such as, digital gear cooling, in the plan of the nuclear reactor, manage of heating and air flow in constructing design, and insulation of plane cabin, and so on. The Boussinesq models are utilized to understand this perception. In the Boussinesq guess, density varies with heat difference. Later, Astanina et al. [64] discussed numerical study of Natural convection MHD fluid flow with entropy optimization.

The boundary layer along material transports, glass fibre creation, hot rolling, and plastic film drawing are among the most fundamental peculiarities that have gained recognition from researchers. Following a thorough research, they discovered that the majority of the fundamentally designed process necessitates the use of a stretching sheet. Sulemana et al. [91] discussed the boundary layer fluid flow over stretching vertical surface.

## 7.2 Novelty of the Chapter

In light of the above studies, the aim of this investigation is to analyze joule heating, nonlinear radiation and viscous dissipation effects on unsteady Natural convective flow of MHD williamson fluid across a stretching sheet. Convective boundary conditions, slip effect and entropy generation rate are included in this investigation.

### 7.3 Mathematical Formulation of the Problem

It is assumed that two dimensional, unsteady flow of an incompressible Williamson fluid across a stretching sheet with joule heating, nonlinear radiation and viscous dissipation have been considered. Entropy generation rate is discussed here. The slip condition and convective boundary conditions have been addressed. As seen in Figure 7.1 the vertical axis was chosen transverse to the stretching sheet. Stretching sheet is taken along  $x$  axis. Non-uniform velocity of the sheet is  $U_w(x, t) = \frac{bx}{1-\alpha t}$ , where  $b$  is the rate of stretching sheet with respect to  $x$  axis where  $\alpha t$  is a positive constant according to case  $\alpha t < 1$ . Where  $\mathcal{B} = B_0/\sqrt{1-\alpha t}$  is the magnetic field's strength and is applied in the direction of the positive  $y$  axis, Comparing the magnetic Reynolds number to the induced magnetic field, it is very small.

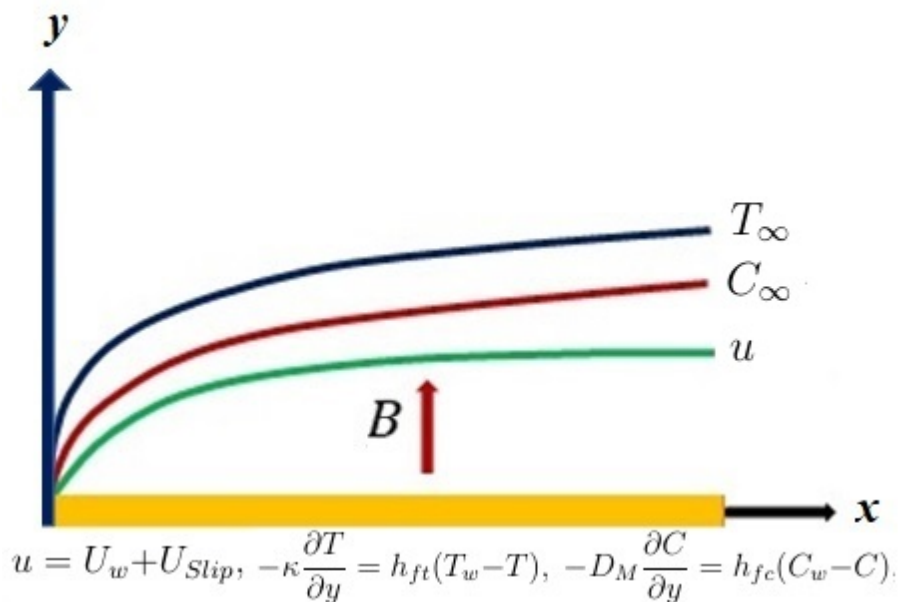


Figure 7.1: Physical Sketch of the Problem

Governing equations for Williamson fluid are as follows:

$$\frac{\partial u}{\partial x} + \frac{\partial v}{\partial y} = 0, \quad (7.3.1)$$

$$\frac{\partial u}{\partial t} + u \frac{\partial u}{\partial x} + v \frac{\partial u}{\partial y} = \nu \frac{\partial^2 u}{\partial y^2} + \sqrt{2}\Gamma\nu \frac{\partial^2 u}{\partial y^2} \frac{\partial u}{\partial y} - \frac{\sigma \mathcal{B}^2}{\rho} u + g\beta_C(C - C_\infty) + g\beta_T(T - T_\infty), \quad (7.3.2)$$

$$\frac{\partial T}{\partial t} + u \frac{\partial T}{\partial x} + v \frac{\partial T}{\partial y} = \frac{\kappa}{\rho C_p} \frac{\partial^2 T}{\partial y^2} - \frac{1}{\rho C_p} \frac{\partial q_r}{\partial y} + \frac{\sigma \mathcal{B}^2}{\rho C_p} u^2 + \frac{\mu}{\rho C_p} \left( \frac{\partial u}{\partial y} \right)^2, \quad (7.3.3)$$

$$\frac{\partial C}{\partial t} + u \frac{\partial C}{\partial x} + v \frac{\partial C}{\partial y} = D_M \frac{\partial^2 C}{\partial y^2} + k_c(C - C_\infty), \quad (7.3.4)$$

where  $u$  is the velocity components along the  $x$ -axis and  $v$  with the  $y$ -axis, respectively.  $\beta_T$ ,  $\beta_C$ ,  $g$  and  $\Gamma$  are thermal expansion coefficient, concentration expansion coefficient, gravity and time fluid parameter respectively.  $T_w$  and  $C_w$  symbolizes surface temperature and concentration, respectively.  $D_M$  and  $k_c$  are mass diffusivity and reaction rate constant. Linearized Heat flux by Rosseland [126] is:

$$q_r = -\frac{16\sigma^*T_\infty^3}{3k^*} \frac{\partial T}{\partial y}, \quad (7.3.5)$$

where  $k^*$  and  $\sigma^*$  are mean absorption coefficient and Stefan-Boltzmann constant respectively. In light of the necessity of nonlinear irradiation, we convert  $T_\infty^3$  with  $T^3$  in Equation (7.3.6), then

$$q_r = -\frac{16\sigma^*T^3}{3k^*} \frac{\partial T}{\partial y}, \quad (7.3.6)$$

The mathematical model has the following boundary conditions

$$u = U_w + U_{Slip}, \quad v = v_w = \frac{v_0}{\sqrt{1 - \alpha t}}, \quad -\kappa \frac{\partial T}{\partial y} = h_{ft}(T_w - T), \\ -D_M \frac{\partial C}{\partial y} = h_{fc}(C_w - C), \quad \text{at } y = 0, \quad (7.3.7)$$

$$u \rightarrow 0, \quad T \rightarrow T_\infty, C \rightarrow C_\infty, \quad \text{as } y \rightarrow \infty. \quad (7.3.8)$$

Introducing the following transformation to convert equations (7.3.1)-(7.3.4) and equation (7.3.7)-(7.3.8) into nonlinear ordinary differential equations,

$$\eta = \sqrt{\frac{b}{\nu(1 - \alpha t)}}y, \quad u = \frac{bx}{(1 - \alpha t)}f'(\eta), \quad v = -\sqrt{\frac{b\nu}{1 - \alpha t}}f(\eta), \\ B = \frac{B_0}{\sqrt{1 - \alpha t}}, \quad T_w = T_\infty + \frac{b^*x}{(1 - \alpha t)^2}, \quad C_w = C_\infty + \frac{c^*x}{(1 - \alpha t)^2}, \\ T = T_\infty + \frac{b^*x}{(1 - \alpha t)^2}\theta(\eta), \quad C = C_\infty + \frac{c^*x}{(1 - \alpha t)^2}\phi(\eta), \quad (7.3.9)$$

Using the similarity variables above Equation (7.3.1) is fulfilled. Equations (7.3.2)-(7.3.4) and (7.3.7)-(7.3.8) will be converted into the following nonlinear ordinary differential equations:

$$f'''(1 + We f'') + f f'' - M f' + Gr_T \theta + Gr_C \phi - f' f' - A \left[ f' + \left(\frac{\eta}{2}\right) f'' \right] = 0, \quad (7.3.10)$$

$$\left(1 + \frac{4}{3}Rd \{1 + (\theta_w - 1)\theta\}^3\right) \theta'' + 4Rd \{1 + (\theta_w - 1)\theta\}^2 (\theta_w - 1)\theta'^2 + Pr \left[ Ec f''^2 + Ec M f'^2 - f'\theta + f\theta' - 2A \left\{ \theta + \left(\frac{\eta}{4}\right) \theta' \right\} \right] = 0, \quad (7.3.11)$$

$$\phi'' + Sc \left[ \phi' f - f' \phi - K_c \phi - 2A \left\{ \phi + \left(\frac{\eta}{4}\right) \phi' \right\} \right] = 0, \quad (7.3.12)$$

with

$$f(0) = f_w, \quad f'(0) = 1 + \gamma f''(0), \quad \theta'(0) = \lambda_1(\theta(0) - 1), \\ \phi'(0) = \lambda_2(\phi(0) - 1), \quad \theta(\infty) = f'(\infty) = \phi(\infty) = 0. \quad (7.3.13)$$

where  $We = \sqrt{\frac{2\Gamma^2 b^3 x^2}{\nu(1-\alpha t)^3}}$ ,  $Pr = \frac{\mu C_p}{\kappa}$ ,  $M = \frac{\sigma B_0^2}{\rho b}$ ,  $\theta_w = \frac{T_w}{T_\infty}$ ,  $Rd = \frac{4\sigma^* T_\infty^3}{k^* \kappa}$ ,  $Gr_T = \frac{gb^* \beta_T}{b^2}$ ,  $Sc = \frac{\nu}{D_M}$ ,  $Gr_C = \frac{gc^* \beta_C}{b^2}$ ,  $A = \frac{\alpha}{b}$ ,  $Ec = \frac{b^2 x}{b^* C_p}$ ,  $f_w = -\frac{v_0}{\sqrt{b\nu}}$ ,  $K_c = \frac{k_c}{b}$ ,  $\gamma = \alpha\mu\sqrt{\frac{b}{\nu(1-\alpha t)}}$ ,  $\lambda_1 = -\frac{h_{ft}}{\kappa}\sqrt{\frac{\nu(1-\alpha t)}{b}}$  and  $\lambda_2 = -\frac{h_{fc}}{D_M}\sqrt{\frac{\nu(1-\alpha t)}{b}}$ .

Skin friction coefficient, rate of heat and mass transfer at the wall are respectively,

$$C_f = \frac{\tau_w}{\rho U_w^2}, \quad Nu = \frac{xq_w}{\kappa(T_w - T_\infty)}, \quad Sh = \frac{xq_m}{D_M(C_w - C_\infty)} \quad (7.3.14)$$

At the wall,  $\tau_w$ ,  $q_m$  and  $q_w$  denote shear stress, mass and heat diffusion respectively, where  $\tau_w$ ,  $q_m$  and  $q_w$  defined as:

$$\tau_w = \mu \left[ \frac{\partial u}{\partial y} + \Gamma \left( \frac{\partial u}{\partial y} \right)^2 \right]_{y=0}, \quad q_w = -\kappa \left( 1 + \frac{16\sigma^* T^3}{3\kappa k^*} \right) \frac{\partial T}{\partial y} \Big|_{y=0}, \quad q_m = -D_M \frac{\partial C}{\partial y} \Big|_{y=0}, \quad (7.3.15)$$

using similarity variables, Skin friction factor, Nusselt and Sherwood numbers

$$C_f (Re_x^{1/2}) = f''(0) + We (f''(0))^2, \quad Sh Re_x^{-1/2} = -\phi'(0), \\ Nu Re_x^{-1/2} = - \left( 1 + \frac{4}{3}Rd \{1 + (\theta_w - 1)\theta(0)\}^3 \right) \theta'(0), \quad (7.3.16)$$

where  $Re_x = \frac{bx^2}{\nu(1-\alpha t)}$  is local Reynolds number.

Generation of entropy is

$$S_G = \underbrace{\frac{\kappa}{T_\infty^2} \left(1 + \frac{16\sigma^* T^3}{3\kappa k^*}\right) \left(\frac{\partial T}{\partial y}\right)^2}_{\text{heat transfer irreversibility}} + \underbrace{\frac{\mu}{T_\infty} \left(\frac{\partial u}{\partial y}\right)^2}_{\text{viscous dissipation irreversibility}} + \underbrace{\frac{\sigma B_0^2 u^2}{T_\infty}}_{\text{Joule heating irreversibility}} + \underbrace{\frac{RD}{C_\infty} \left(\frac{\partial C}{\partial y}\right)^2}_{\text{mass transfer irreversibility}} \quad (7.3.17)$$

Applying similarity variables, we get

$$N_G = \alpha_1 \left(1 + \frac{4}{3} Rd \{1 + (\theta_w - 1)\theta\}^3\right) \theta'^2 + Br f'^2 + M Br f'^2 + \left(\frac{L^*}{\alpha_1}\right) \alpha_2 \phi'^2, \quad (7.3.18)$$

$$\text{Bejan number } Be = \frac{\text{Entropy generation due to heat and mass transfer}}{\text{Total entropy generation}} \quad (7.3.19)$$

then,

$$Be = \frac{\alpha_1 \left(1 + \frac{4}{3} Rd \{1 + (\theta_w - 1)\theta\}^3\right) \theta'^2 + \left(\frac{L^*}{\alpha_1}\right) \alpha_2 \phi'^2}{\alpha_1 \left(1 + \frac{4}{3} Rd \{1 + (\theta_w - 1)\theta\}^3\right) \theta'^2 + Br f'^2 + M Br f'^2 + \left(\frac{L^*}{\alpha_1}\right) \alpha_2 \phi'^2} \quad (7.3.20)$$

$$\text{where } N_G = \frac{T_\infty \nu (1 - \alpha t)}{b \kappa (T_w - T_\infty)} S_G, \quad \alpha_1 = \frac{T_w - T_\infty}{T_\infty}, \quad L^* = \frac{R D C_\infty}{\kappa}, \quad \alpha_2 = \left(\frac{C_w - C_\infty}{C_\infty}\right)^2.$$

## 7.4 Solution by Homotopy Analysis Method

Initial guesses and auxiliary linear operators respectively are

$$f_0(\eta) = f_w + \frac{1}{1 + \gamma} [1 - e^{-\eta}], \quad \theta_0(\eta) = \frac{\lambda_1}{1 + \lambda_1} e^{-\eta}, \quad \phi_0(\eta) = \frac{\lambda_2}{1 + \lambda_2} e^{-\eta}, \quad (7.4.1)$$

$$\mathcal{L}_f = \frac{\partial^3 f}{\partial \eta^3} - \frac{\partial f}{\partial \eta}, \quad \mathcal{L}_\theta = \frac{\partial^2 \theta}{\partial \eta^2} - \theta, \quad \mathcal{L}_\phi = \frac{\partial^2 \phi}{\partial \eta^2} - \phi, \quad (7.4.2)$$

where  $\mathcal{L}_f(k_1 + k_2 e^\eta + k_3 e^{-\eta}) = 0$ ,  $\mathcal{L}_\theta(k_4 + k_5 e^{-\eta}) = 0$ ,  $\mathcal{L}_\phi(k_6 + k_7 e^{-\eta}) = 0$ , and  $k_1, k_2, \dots, k_7$  are arbitrary constants.

### 7.4.1 Zero-th order deformation

$$(1 - q) \mathcal{L}_f [F(\eta; q) - f_0(\eta)] = \hbar_f q \mathcal{N}_f [F(\eta; q)], \quad (7.4.3)$$

$$(1 - q) \mathcal{L}_\theta [\Theta(\eta; q) - \theta_0(\eta)] = \hbar_\theta q \mathcal{N}_\theta [\Theta(\eta; q)], \quad (7.4.4)$$

$$(1 - q) \mathcal{L}_\phi [\Phi(\eta; q) - \phi_0(\eta)] = \hbar_\phi q \mathcal{N}_\phi [\Phi(\eta; q)], \quad (7.4.5)$$

where

$$\begin{aligned} \mathcal{N}_f [F (\eta; q)] = & \left( 1 + We \frac{\partial^2 F}{\partial \eta^2} \right) \frac{\partial^3 F}{\partial \eta^3} - M \frac{\partial F}{\partial \eta} + Gr_T \Theta - \left( \frac{\partial F}{\partial \eta} \right)^2 + Gr_C \Phi \\ & + F \frac{\partial^2 F}{\partial \eta^2} - A \left( \frac{\partial F}{\partial \eta} + \frac{\eta}{2} \frac{\partial^2 F}{\partial \eta^2} \right), \end{aligned} \quad (7.4.6)$$

$$\begin{aligned} \mathcal{N}_\theta [\Theta (\eta; q)] = & \left( 1 + \frac{4}{3} Rd \{ 1 + (\theta_w - 1) \Theta \}^3 \right) \frac{\partial^2 \Theta}{\partial \eta^2} - Pr \frac{\partial F}{\partial \eta} \Theta + Pr Ec \left( \frac{\partial^2 F}{\partial \eta^2} \right)^2 \\ & + 4Rd \{ 1 + (\theta_w - 1) \Theta \}^2 (\theta_w - 1) \left( \frac{\partial \Theta}{\partial \eta} \right)^2 + PrMEc \left( \frac{\partial F}{\partial \eta} \right)^2 + PrF \frac{\partial \Theta}{\partial \eta} \\ & - 2APr \left( \Theta + \frac{\eta}{4} \frac{\partial \Theta}{\partial \eta} \right), \end{aligned} \quad (7.4.7)$$

$$\mathcal{N}_\phi [\Phi (\eta; q)] = \frac{\partial^2 \Phi}{\partial \eta^2} + Sc \left[ F \frac{\partial \Phi}{\partial \eta} - \frac{\partial F}{\partial \eta} \Phi - K_c \Phi - 2A \left( \Phi + \frac{\eta}{4} \frac{\partial \Phi}{\partial \eta} \right) \right], \quad (7.4.8)$$

Boundary conditions subject to

$$\begin{aligned} F (0; q) = f_w, \quad F' (0; q) = 1 + \gamma F'' (0; q), \quad F' (+\infty; q) = 0, \\ \Theta' (0; q) = \lambda_1 (\Theta (0; q) - 1), \quad \Theta (+\infty; q) = 0, \\ \Phi' (0; q) = \lambda_2 (\Phi (0; q) - 1), \quad \Phi (+\infty; q) = 0, \end{aligned} \quad (7.4.9)$$

Hence in terms of  $q$  and  $\eta$ ,  $F (\eta; q)$ ,  $\Theta (\eta; q)$  and  $\Phi (\eta; q)$  are unknown functions. The nonlinear operators with the non-zero auxiliary parameters are respectively denoted by  $\mathcal{h}_f$ ,  $\mathcal{h}_\theta$ ,  $\mathcal{h}_\phi$ ,  $\mathcal{N}_f$ ,  $\mathcal{N}_\theta$  and  $\mathcal{N}_\phi$ . Additionally, embedding parameter is  $q \in (0, 1)$  is when  $q = 0$  and  $q = 1$ , then

$$\left. \begin{aligned} F (\eta; 0) = f_0 (\eta), \quad F (\eta; 1) = f (\eta), \\ \Theta (\eta; 0) = \theta_0 (\eta), \quad \Theta (\eta; 1) = \theta (\eta), \\ \Phi (\eta; 0) = \phi_0 (\eta), \quad \Phi (\eta; 1) = \phi (\eta), \end{aligned} \right\} \quad (7.4.10)$$

when  $q$  fluctuates between 0 to 1, the variation will be  $F(\eta; q)$ ,  $\Theta(\eta; q)$  and  $\Phi(\eta; q)$  differ from  $f_0(\eta)$ ,  $\theta_0(\eta)$  and  $\phi_0(\eta)$  to  $f(\eta)$ ,  $\theta(\eta)$ , and  $\phi(\eta)$ . So, we get

$$\left. \begin{aligned} F(\eta; q) &= f_0(\eta) + \sum_{i=1}^{\infty} q^i f_i(\eta) \\ \Theta(\eta; q) &= \theta_0(\eta) + \sum_{i=1}^{\infty} q^i \theta_i(\eta), \\ \Phi(\eta; q) &= \phi_0(\eta) + \sum_{i=1}^{\infty} q^i \phi_i(\eta) \end{aligned} \right\} \quad (7.4.11)$$

where  $f_i(\eta) = \frac{1}{i!} \frac{\partial^i f(\eta; q)}{\partial \eta^i} \Big|_{q=0}$ ,  $\theta_i(\eta) = \frac{1}{i!} \frac{\partial^i \theta(\eta; q)}{\partial \eta^i} \Big|_{q=0}$ ,  $\phi_i(\eta) = \frac{1}{i!} \frac{\partial^i \phi(\eta; q)}{\partial \eta^i} \Big|_{q=0}$ ,

Convergence of the series depends heavily on  $\hbar_f$ ,  $\hbar_\theta$  and  $\hbar_\phi$ . For proper values of  $\hbar_f$ ,  $\hbar_\theta$  and  $\hbar_\phi$ , equation (7.4.11) is converging at  $q = 1$ . Thus, we get

$$\left. \begin{aligned} f(\eta) &= f_0(\eta) + \sum_{i=1}^{\infty} f_i(\eta) \\ \theta(\eta) &= \theta_0(\eta) + \sum_{i=1}^{\infty} \theta_i(\eta), \\ \phi(\eta) &= \phi_0(\eta) + \sum_{i=1}^{\infty} \phi_i(\eta) \end{aligned} \right\} \quad (7.4.12)$$

## 7.4.2 i-th order equation

$i^{\text{th}}$  order deformation equations are

$$\left. \begin{aligned} \mathcal{L}_f [f_i(\eta) - \chi_i f_{i-1}(\eta)] &= \hbar_f \mathcal{R}_{f, i}(\eta), \\ \mathcal{L}_\theta [\theta_i(\eta) - \chi_i \theta_{i-1}(\eta)] &= \hbar_\theta \mathcal{R}_{\theta, i}(\eta), \\ \mathcal{L}_\phi [\phi_i(\eta) - \chi_i \phi_{i-1}(\eta)] &= \hbar_\phi \mathcal{R}_{\phi, i}(\eta), \end{aligned} \right\} \quad (7.4.13)$$

with

$$\begin{aligned} f_i(0) = 0, \quad f'_i(0) = \gamma f''_i(0), \quad f'_i(+\infty) = 0, \quad \theta'_i(0) = \lambda_1 \theta''_i(0), \quad \phi'_i(0) = \lambda_2 \phi''_i(0), \\ \theta_i(+\infty) = 0, \quad \phi_i(0) = 0. \end{aligned} \quad (7.4.14)$$

$$\begin{aligned} \mathcal{R}_{f,i}(\eta) = & f_{i-1}''' + We \sum_{j=0}^{i-1} f_{i-1-j}''' f_j'' + \sum_{j=0}^{i-1} f_{i-1-j}'' f_j' - \sum_{j=0}^{i-1} f_{i-1-j}' f_j' - M f_{i-1}' \\ & + Gr_T \theta_{i-1} + Gr_C \phi_{i-1} - A \left( f_{i-1}' + \frac{\eta}{2} f_{i-1}'' \right) \end{aligned} \quad (7.4.15)$$

$$\begin{aligned} \mathcal{R}_{\theta,i}(\eta) = & \frac{4}{3} Rd (\theta_w - 1)^3 \left\{ \sum_{j=0}^{i-1} \theta_{i-1-j}'' \sum_{l=0}^j \theta_{j-l} \sum_{p=0}^l \theta_{l-p} \theta_p \right\} + \left( 1 + \frac{4}{3} Rd \right) \theta_{i-1}'' \\ & + 4Rd (\theta_w - 1)^3 \left\{ \sum_{j=0}^{i-1} \theta_{i-1-j}' \sum_{l=0}^j \theta_{j-l}' \sum_{p=0}^l \theta_{l-p} \theta_p \right\} + Pr \sum_{j=0}^{i-1} \theta_{i-1-j}' f_j \\ & + 4Rd (\theta_w - 1) \sum_{j=0}^{i-1} \theta_{i-1-j}'' \theta_j + 4Rd (\theta_w - 1)^2 \sum_{j=0}^{i-1} \theta_{i-1-j}'' \sum_{l=0}^j \theta_{j-l} \theta_l \\ & + 4Rd (\theta_w - 1) \sum_{j=0}^{i-1} \theta_{i-1-j}' \theta_j' + 8Rd (\theta_w - 1)^2 \sum_{j=0}^{i-1} \theta_{i-1-j}' \sum_{l=0}^j \theta_{j-l}' \theta_l \\ & + PrEc \sum_{j=0}^{i-1} f_{i-1-j}'' f_j'' + PrMEc \sum_{j=0}^{i-1} f_{i-1-j}' f_j' - Pr \sum_{j=0}^{i-1} f_{i-1-j}' \theta_j \\ & - 2PrA \left( \theta_{i-1} + \frac{\eta}{2} \theta_{i-1}' \right) \end{aligned} \quad (7.4.16)$$

$$\mathcal{R}_{\phi,i}(\eta) = \phi_{i-1}'' + Sc \left[ \sum_{j=0}^{i-1} f_{i-1-j} \phi_j' - \sum_{j=0}^{i-1} f_{i-1-j}' \phi_j - K_c \phi_j - 2A \left( \phi_{i-1} + \frac{\eta}{4} \phi_{i-1}' \right) \right] \quad (7.4.17)$$

with

$$\chi_i = \begin{cases} 0, & i < 1 \\ 1, & i \geq 1 \end{cases} \quad (7.4.18)$$

The general solutions of equation (7.4.13) is given by

$$\left. \begin{aligned} f_i(\eta) &= f_i^*(\eta) + k_1 + k_2 e^\eta + k_3 e^{-\eta} \\ \theta_i(\eta) &= \theta_i^*(\eta) + k_4 + k_5 e^{-\eta} \\ \phi_i(\eta) &= \phi_i^*(\eta) + k_6 + k_7 e^{-\eta} \end{aligned} \right\} \quad (7.4.19)$$

where the constants  $k_j$ , ( $j = 1, 2, \dots, 7$ ) can be found by the boundary conditions.

### 7.4.3 Convergence Analysis

It is vital to make sure that our series solution converges while using the HAM approach. The value of the auxiliary parameter  $\hbar$  has a massive effect on the HAM

solution's approximation convergence rate. We have a lot of flexibility in monitoring and modifying convergence zone of the series solution because to this auxiliary parameter.  $f''(0)$ ,  $\theta'(0)$  and  $\phi'(0)$  are plotted at the 20<sup>th</sup> order of approximations to find the acceptable values of  $\hbar_f$ ,  $\hbar_\theta$  and  $\hbar_\phi$ . The selection of the values for  $\hbar_f$ ,  $\hbar_\theta$  and  $\hbar_\phi$  ensures that curves are collinear to the horizontal axis. The permissible range for values of  $\hbar_f$  ( $-1.1 < \hbar_f < -0.2$ ),  $\hbar_\theta$  ( $-1.3 < \hbar_\theta < 0.1$ ) and  $\hbar_\phi$  ( $-0.5 < \hbar_\phi < 0.0$ ) is clearly seen in Figure 7.2. Based on the present computations,  $\hbar_f = -0.85$ ,  $\hbar_\theta = -0.94$  and  $\hbar_\phi = -0.34$  are used. Table 7.1 is provided to guarantee the convergence of solutions. The convergence is attained at the 30<sup>th</sup>- order of estimations, as this table clearly demonstrates.

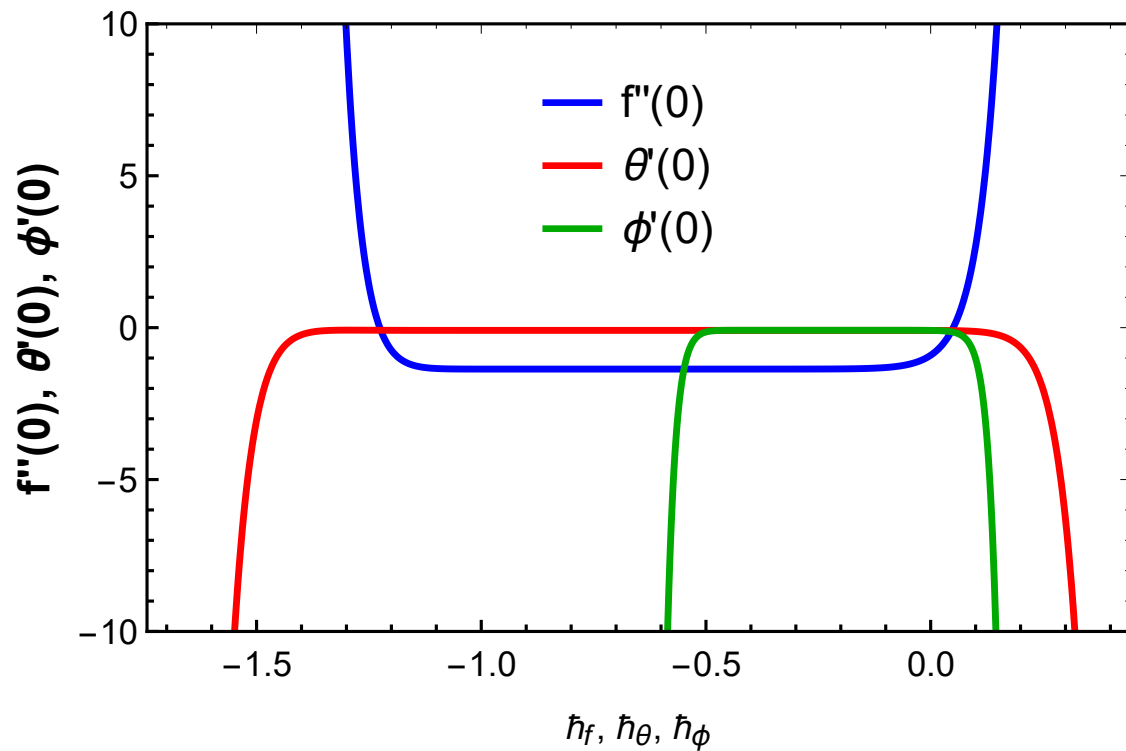


Figure 7.2:  $f''(0)$  for  $\hbar_f$

Table 7.1: Convergence of series solution for  $f''(0)$ ,  $\theta'(0)$  and  $\phi'(0)$  when  $f_w = M = A = Gr_T = Gr_C = 0.5$ ,  $We = \lambda_1 = \lambda_2 = \gamma = K_c = Ec = Rd = 0.1$ ,  $Sc = 0.2$ ,  $Pr = 7.0$ ,  $\theta_w = 1.1$ ,  $h_f = -0.85$ ,  $h_\theta = -0.94$  and  $h_\phi = -0.34$ .

Order of Approximation	$f''(0)$	$-\theta'(0)$	$-\phi'(0)$
1	-1.34652	0.09565	0.08719
5	-1.37864	0.09372	0.08585
10	-1.37848	0.09349	0.08577
15	-1.37834	0.09349	0.08577
20	-1.37835	0.09348	0.08577
25	-1.37835	0.09348	0.08577
30	-1.37835	0.09348	0.08577

## 7.5 Result and Discussion

To provide a physical understanding of unsteady Natural convective flow of Williamson fluid with heat and mass transfer with of viscous dissipation, Joule heating, non-linear radiation effect. Mathematical calculation have been carried out using HAM and influence of pertinent parameters are examined graphically in Figures 7.3-7.25 using Mathematica software.  $f_w = 0.5$ ,  $\lambda_1 = 0.1$ ,  $\lambda_2 = 0.1$ ,  $We = 0.1$ ,  $M = 0.5$ ,  $\gamma = 0.1$ ,  $Pr = 7.0$ ,  $Sc = 0.2$ ,  $A = 0.5$ ,  $Gr_T = 0.5$ ,  $Gr_C = 0.5$ ,  $K_c = 0.1$ ,  $Ec = 0.1$ ,  $Rd = 0.1$ ,  $\theta_w = 1.1$  are taken for calculations. Using all these values graphs and tables are formed otherwise stated. For validity purpose, similarity of the current outcomes of  $f''(0)$  with the previous published result of Yih [62] are explained in Table 7.2. Similarly current outcomes of  $\theta'(0)$  equated with the available published results Ishak [12], Yusof et al. [144], Reddy et al. [87] are explained in Table 7.3 The results shows great agreement so we are confident that the current results are precise.

Figure 7.3 reports the attitudes of the Magnetic parameter  $M$  on the velocity pattern  $f'(\eta)$ . We determined that a decreased velocity corresponds to a Magnetic parameter  $M$ . In this instance, the hydrodynamic case is more compelling than the hydromagnetic one. With a rise in  $M$ , the Lorentz force, which manifests in  $M$ , gets stronger. In actuality, the velocity decays due to the larger Lorentz force. The data of Figure 7.4 depicts the fluid velocity perspective against Weissenberg number  $We$ , and it can be recognized that as Weissenberg number  $We$  improves, the velocity profile shrinks. Weissenberg number's stirring up values boost the relaxation time of the fluid particles, growing viscosity in the procedure. This produces resistance to

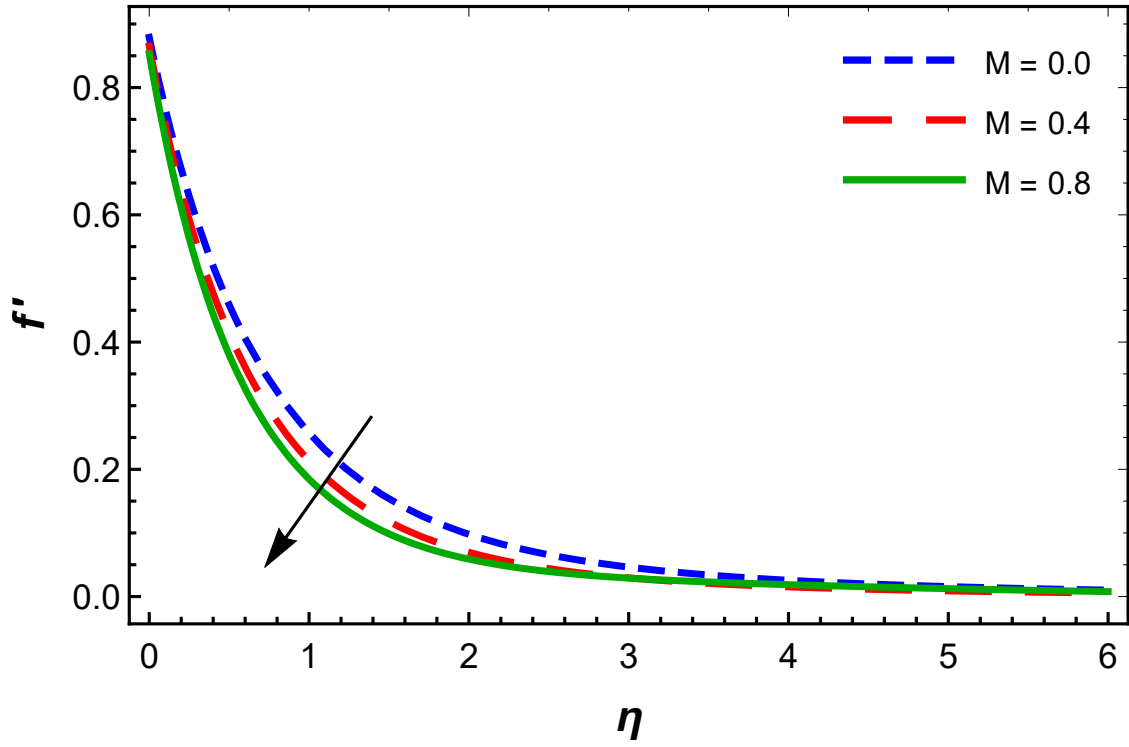
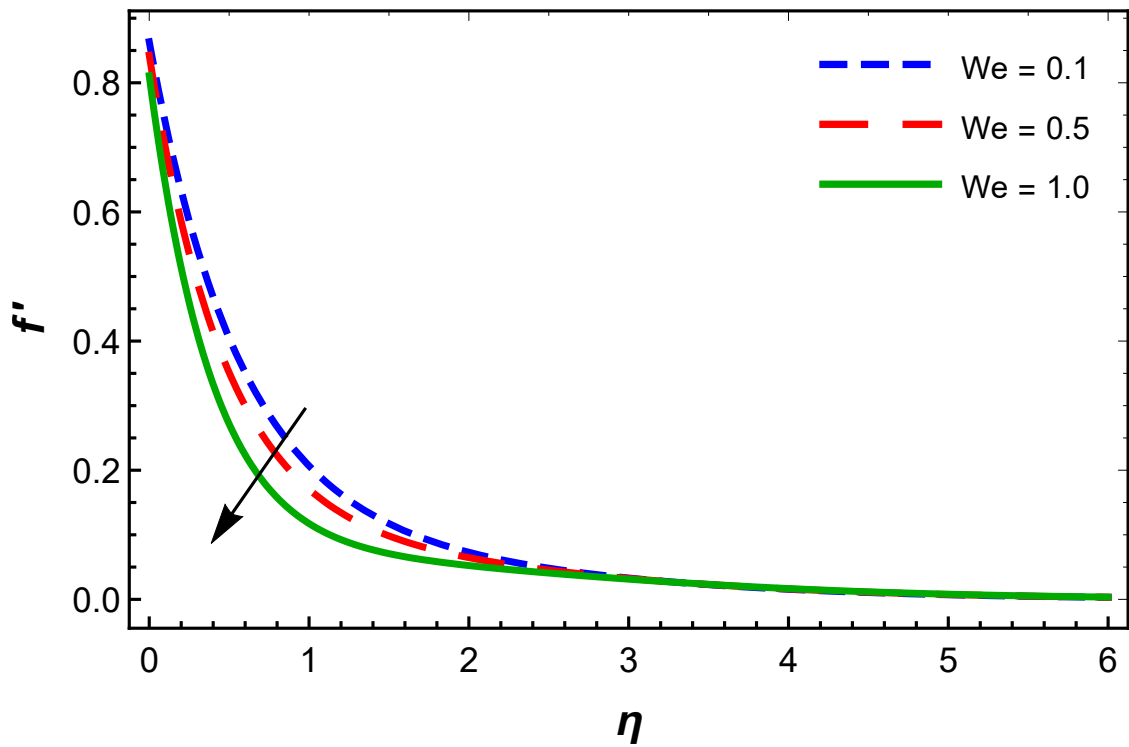
the fluid flow, lowering the velocity of the fluid particles. We can observe in Figures 7.5 and 7.6 that Unsteadiness parameter  $A$  and Suction parameter  $f_w$  have a negative impact on velocity. The Lorentz force, which is a retarding body force introduced by the magnetic field and which increases resistance to transport phenomena. The temperature  $\theta(\eta)$  rises because of the heat that is produced, which can be noticed in the Figure 7.7. The growth in thermal boundary layer development is caused by the enhanced radiative heat transfer to the fluid. As a result, Figure 7.8 demonstrates that temperature goes up as the Radiation parameter  $Rd$  values. Figure 7.9 depicts the temperature distribution for various temperature ratio parameter  $\theta_w$  values. It is evident that the temperature is improved for higher temperature ratio parameter values. The temperature is magnified with growing values of the Eckert number  $Ec$ , depicted in Figure 7.10. The energy produced by the collision of molecules is held in the fluid due to the friction between the molecules, raising the temperature. The significance of the Prandtl number  $Pr$  on the temperature field is shown in Figure 7.11. The temperature of the fluid drops as  $Pr$  raises because the boundary layer thickness is thinner and thermal diffusivity is weaker. Figure 7.12 illustrates the influence of the Unsteadiness parameter  $A$  on the temperature profile. In this case, temperature drops as  $A$  rises. Now, Figure 7.13 evaluated the consequence of the Chemical reaction parameter  $K_c$  on the concentration profile. As  $K_c$  grows, the concentration lowers. Figure 7.14 exhibits how the Schmidt number  $Sc$  affects the concentration field. Because decreasing molecular diffusivity leads in a reduction in the concentration boundary layer, raising  $Sc$  lower the concentration boundary layer. Figure 7.15 indicates in detail how the Unsteadiness parameter affects the concentration profile. In this scenario, concentration falls as  $A$  rises. Figures 7.16 and 7.17 demonstrate how the Bejan number  $Be$  and the rate of entropy generation  $N_G$  both expand as  $L$  grows. Entropy generation develops with raising  $M$  and  $Br$ , as demonstrated in Figures 7.18 and 7.19, although Bejan number has the reverse effect for  $M$  and  $Br$  in Figures 7.20 and 7.21. Figures 7.22 and 7.23 describe the consequences of the  $We$  and the solutal buoyancy parameter on skin friction. We discovered that as both  $We$  and  $Gr_C$  are increased, skin friction increases. Figure 7.24 displays Nusselt number drops for  $\theta_w$  values that increase. Figure 7.25 depicts how the Sherwood number rises as  $K_c$  is raised. Physical quantities for several parameters are provided in Table 7.4.

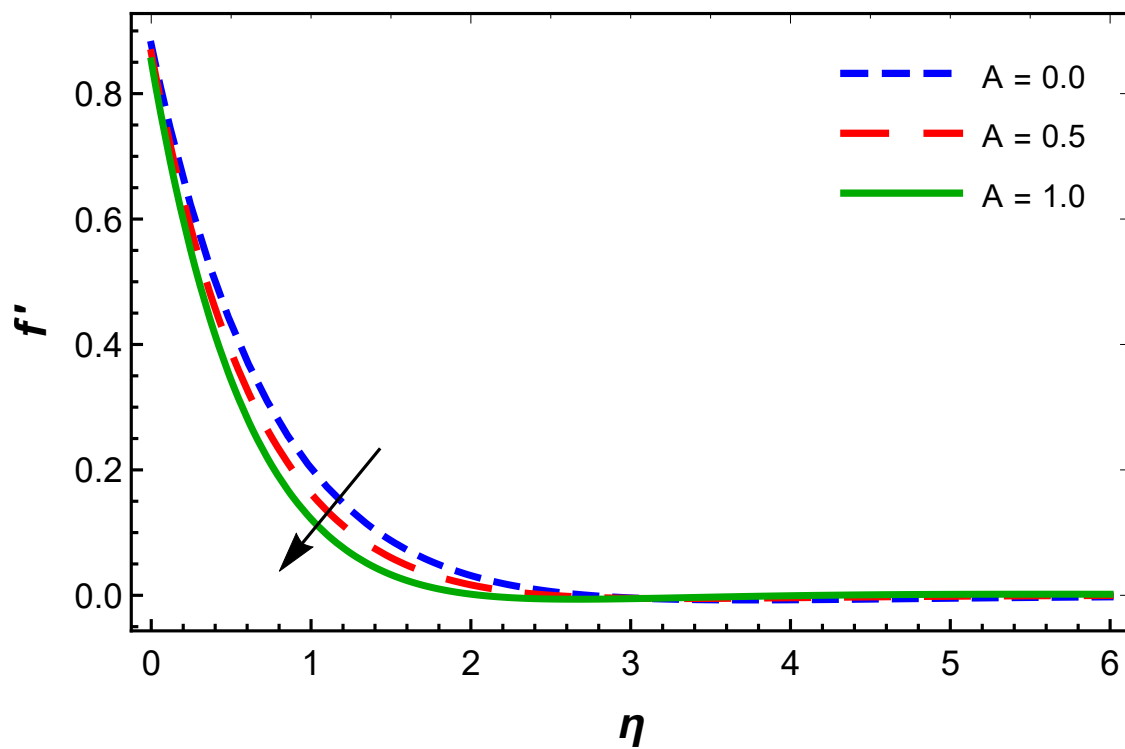
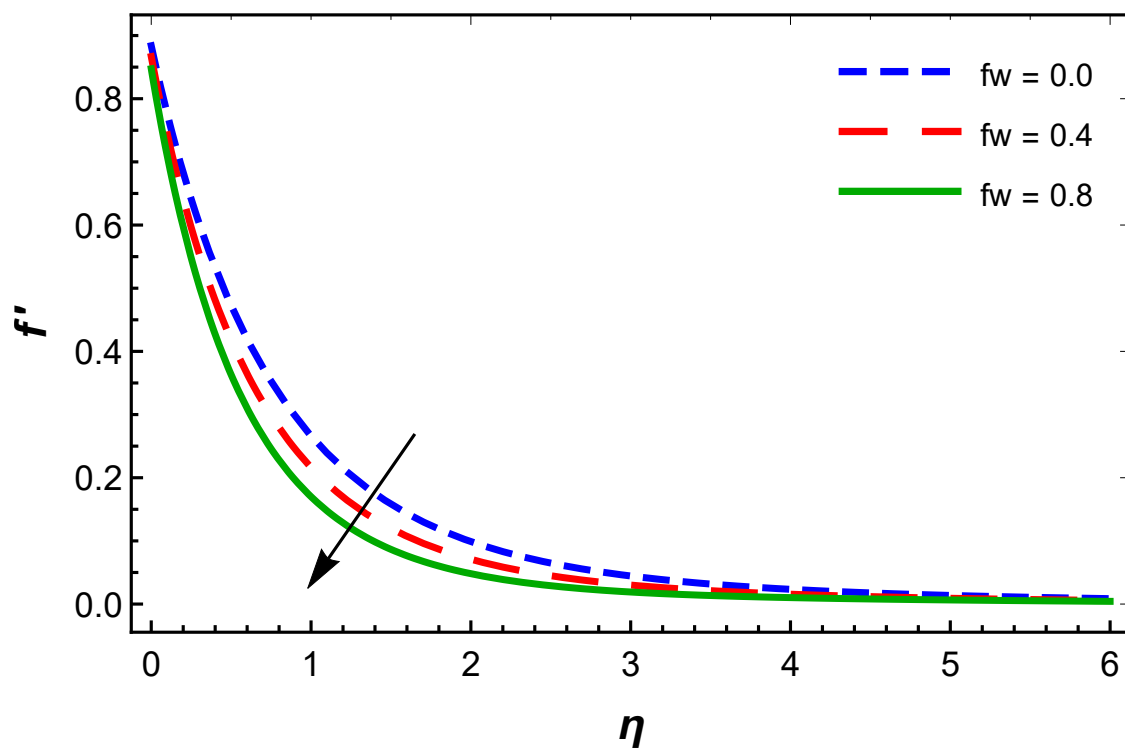
Table 7.2: Similarity of  $f''(0)$  for the different values of  $M$  when  $We = Gr_T = Gr_C = f_w = \gamma = A = 0$ .

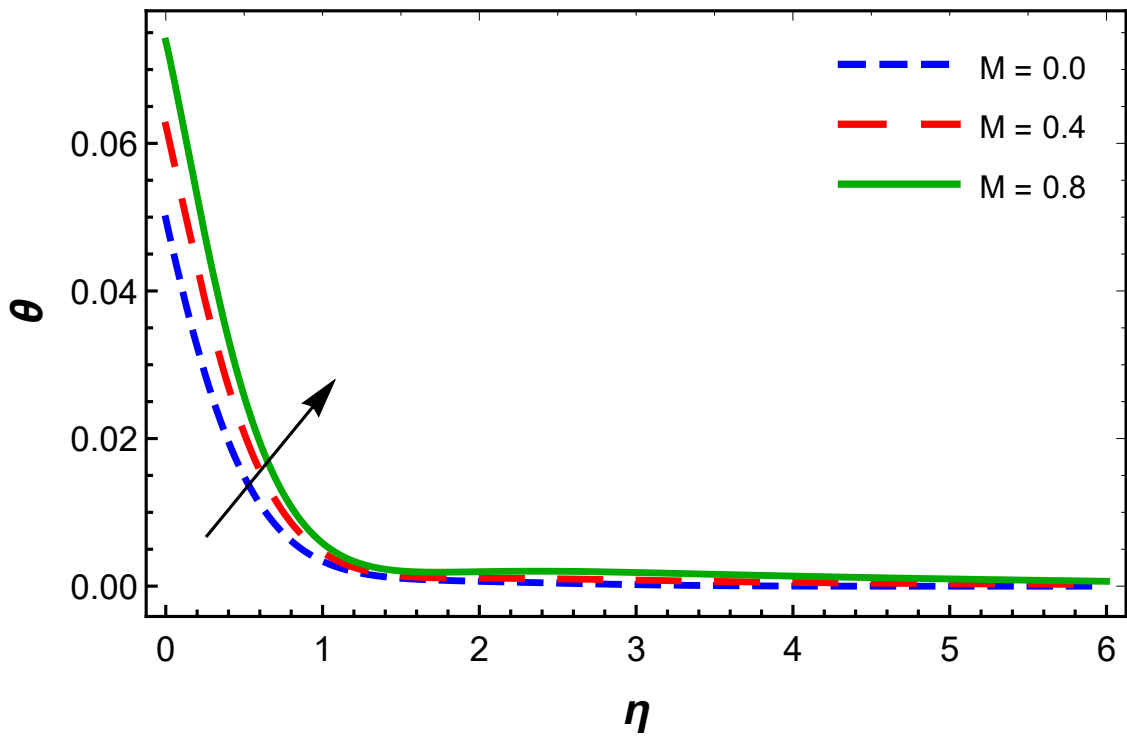
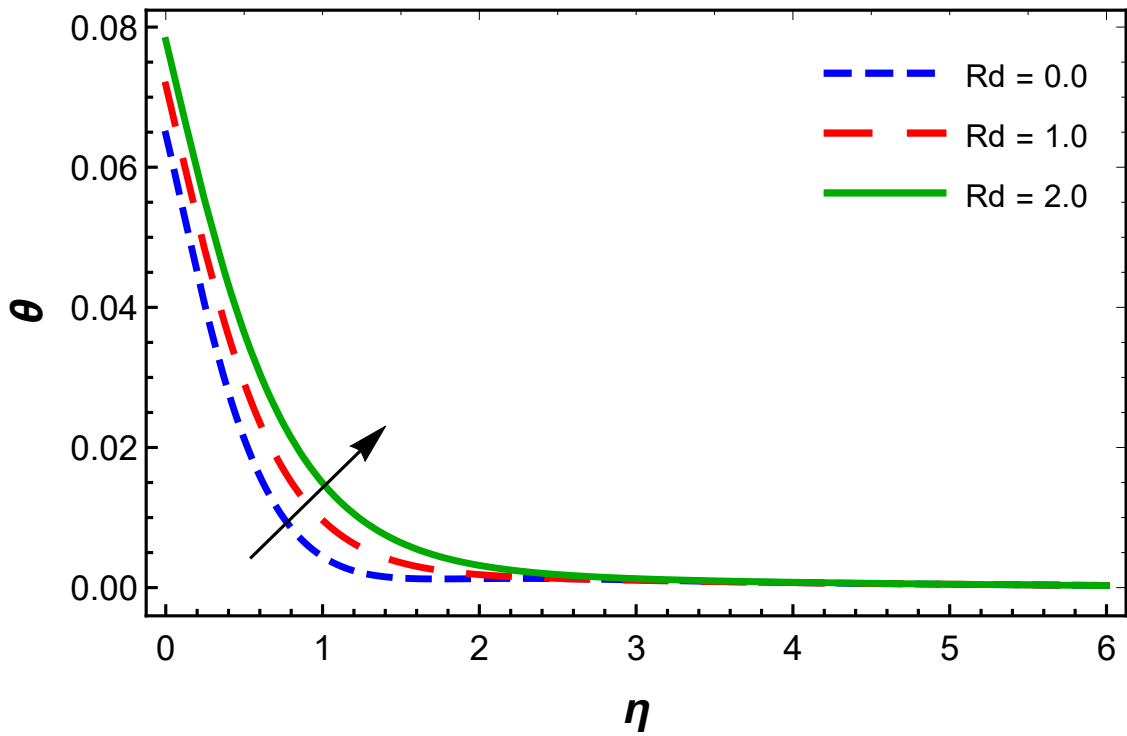
$M$	Yih [62]	Present study
0.0	-1.0000	-1.0000
0.5	-1.2247	-1.2247
1.0	-1.4142	-1.4142
1.5	-1.5811	-1.5811
2.0	-1.7329	-1.7329

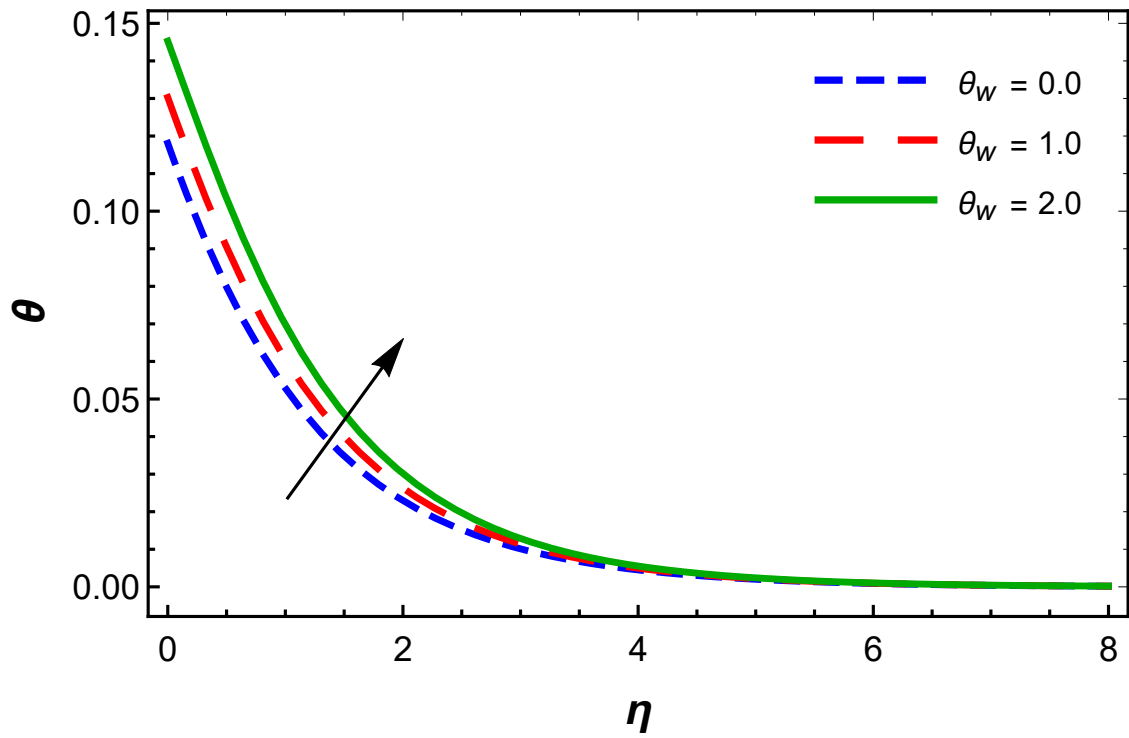
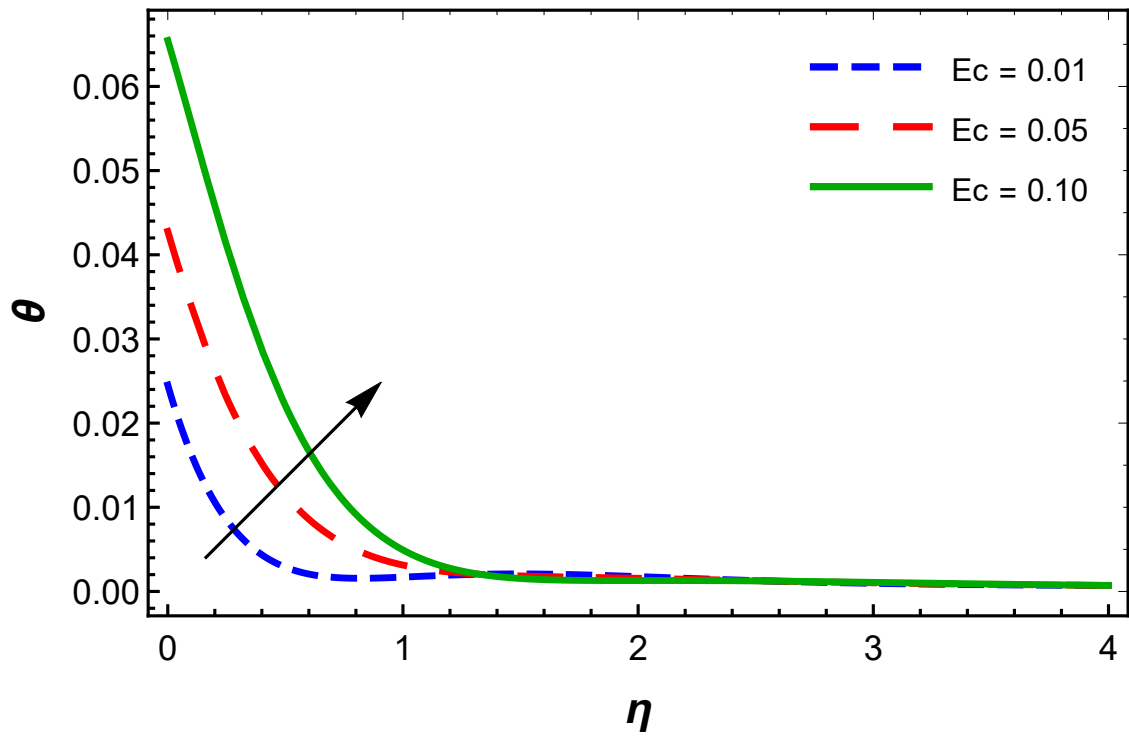
Table 7.3: Similarity of  $-\theta'(0)$  for the different values of  $Pr$  when  $We = M = \theta_w = Rd = Gr_T = Gr_C = Ec = A = \lambda_1 = 0.0$ .

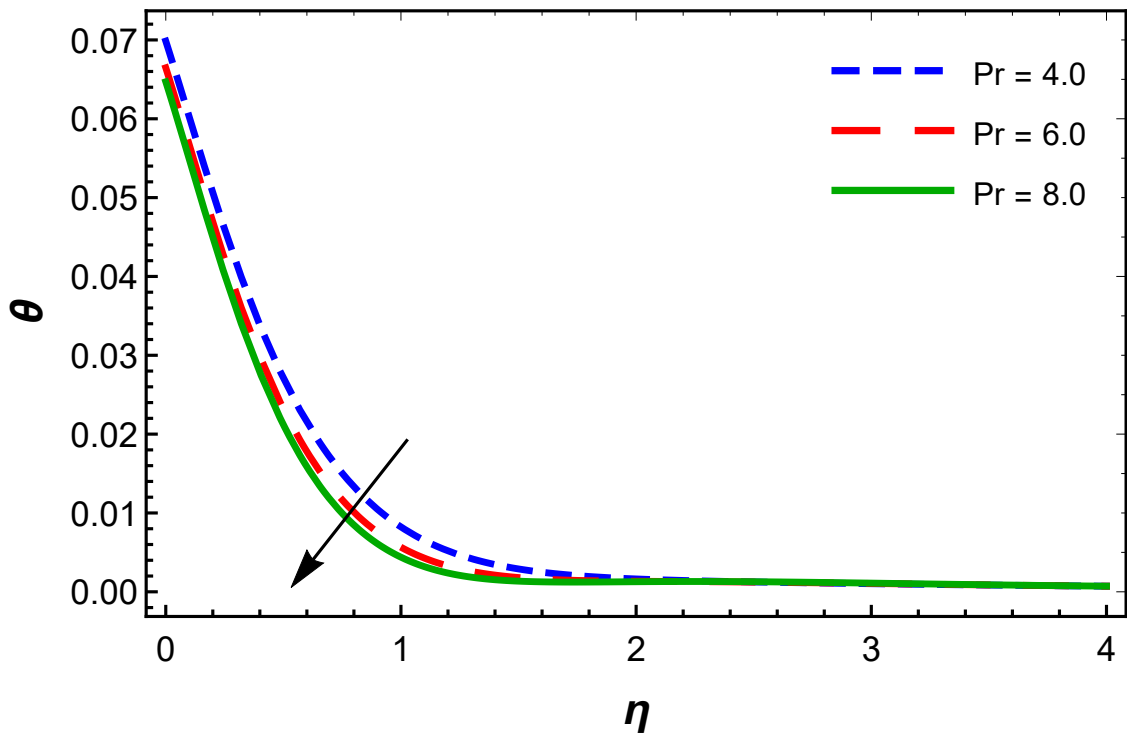
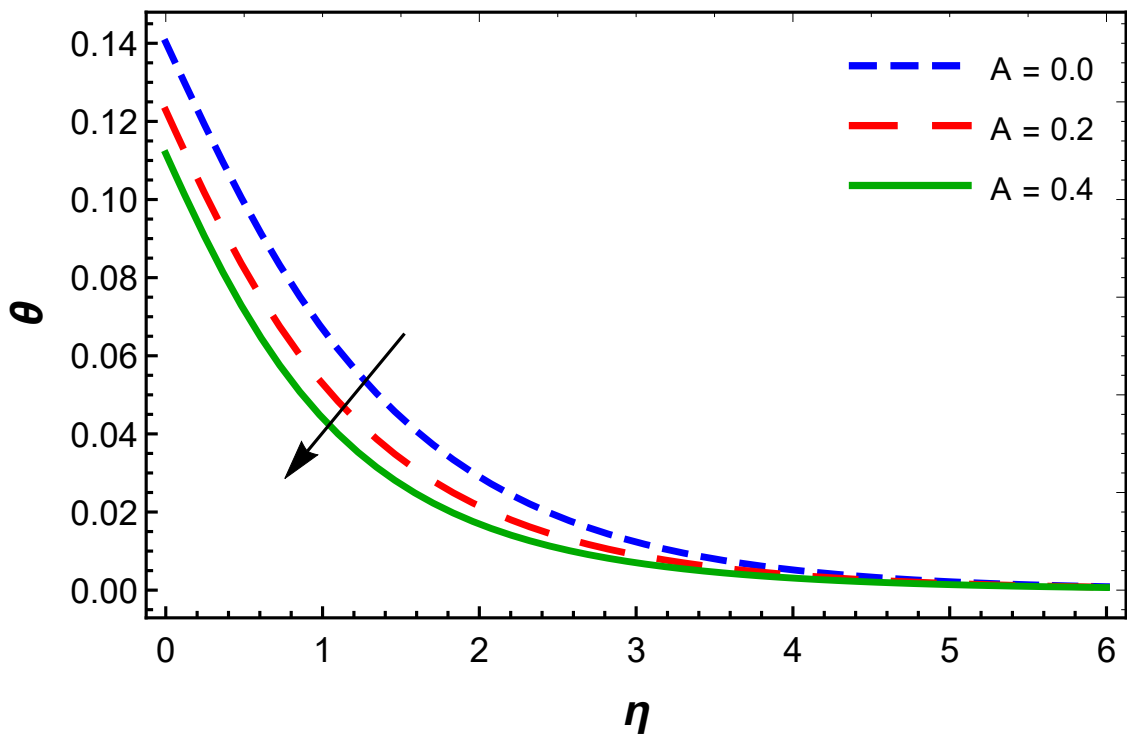
$Pr$	$M$	Ishak [12] Keller box method	Yusof et al. [144] (Runge–Kutta–Fehlberg shooting technique)	Reddy et al. [87] (Keller Box method)	Present
0.72	0	-0.8086	-0.8086	-0.8086	-0.8086
1.0	0	-1.0000	-1.0000	-1.0000	-1.0000
3.0	0	-1.9237	-1.9237	-1.9237	-1.9237
0.7	1.0	-0.6897	-0.6897	-0.6897	-0.6897
1.0	1.0	-0.8921	-0.8921	-0.8921	-0.8921

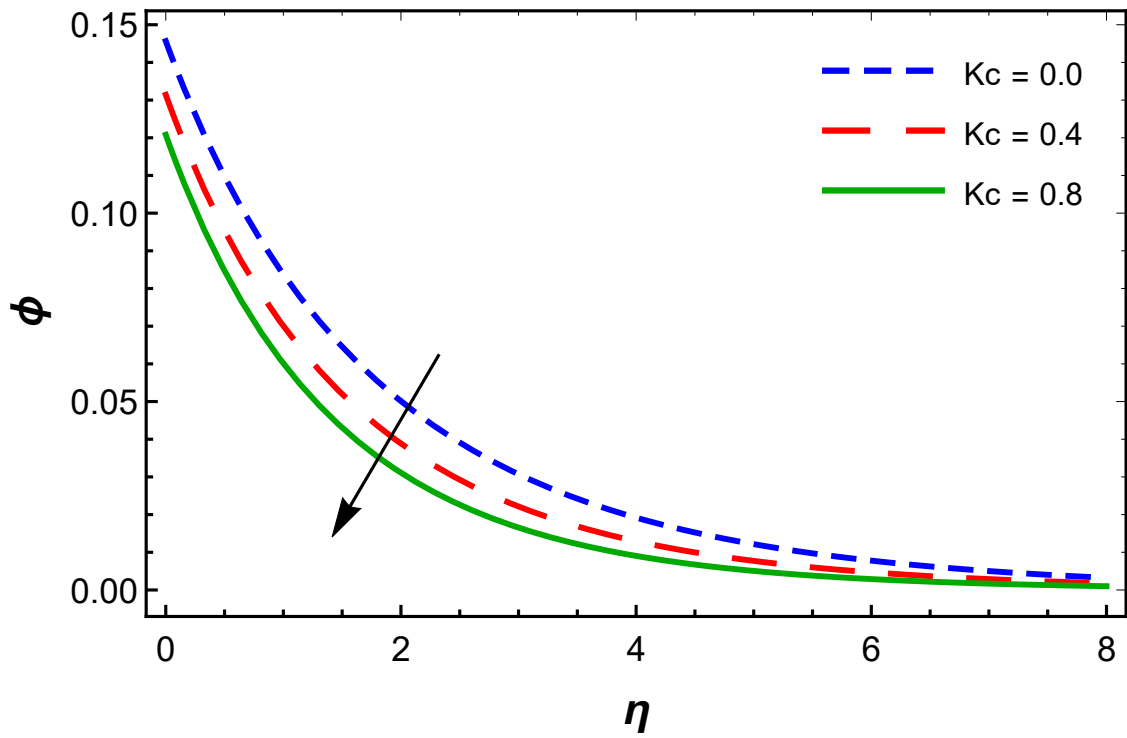
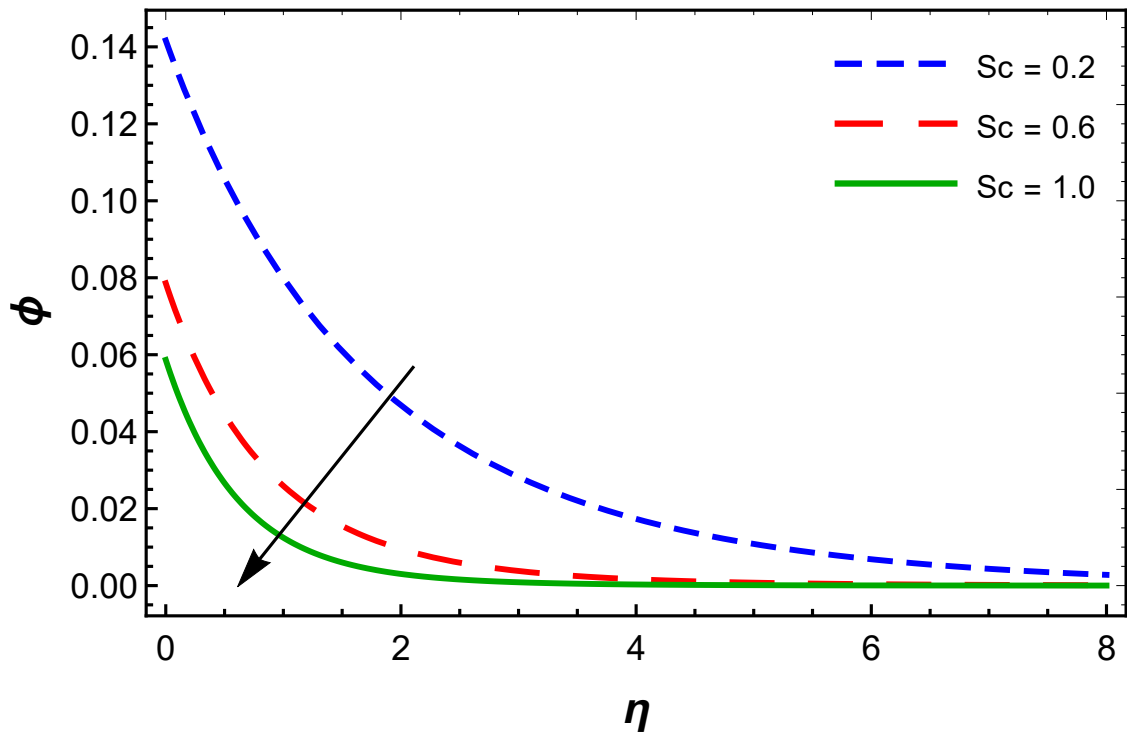
Figure 7.3:  $f'(\eta)$  for  $M$ Figure 7.4:  $f'(\eta)$  for  $We$

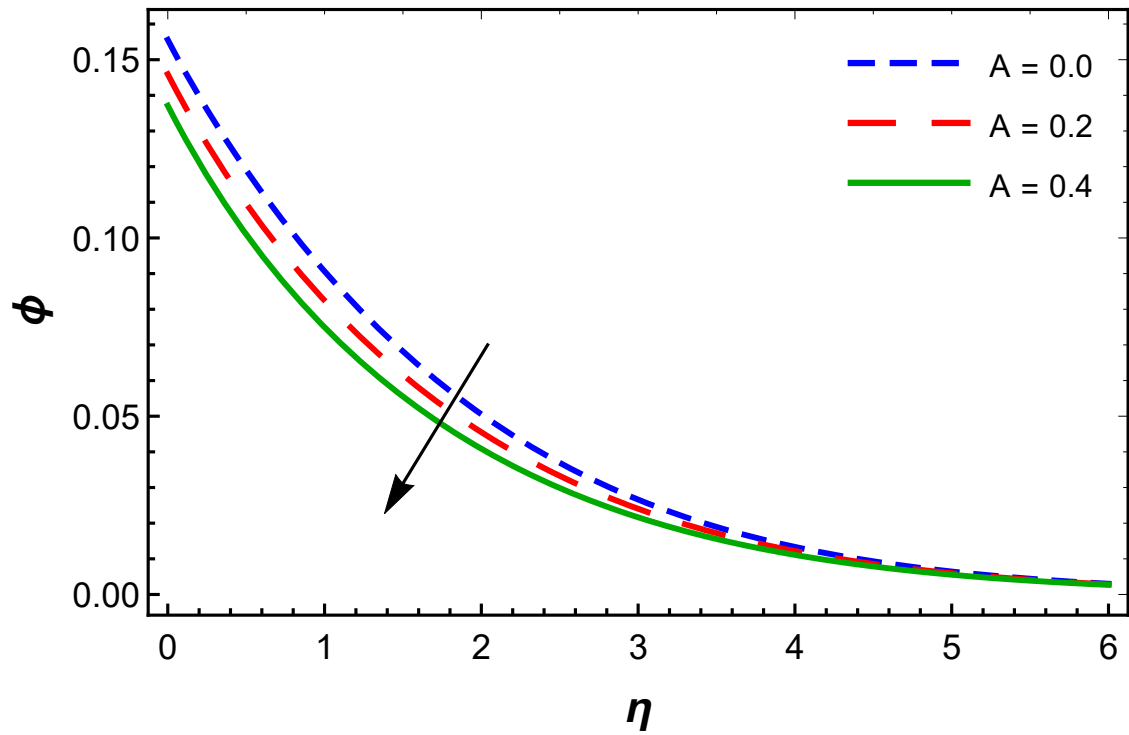
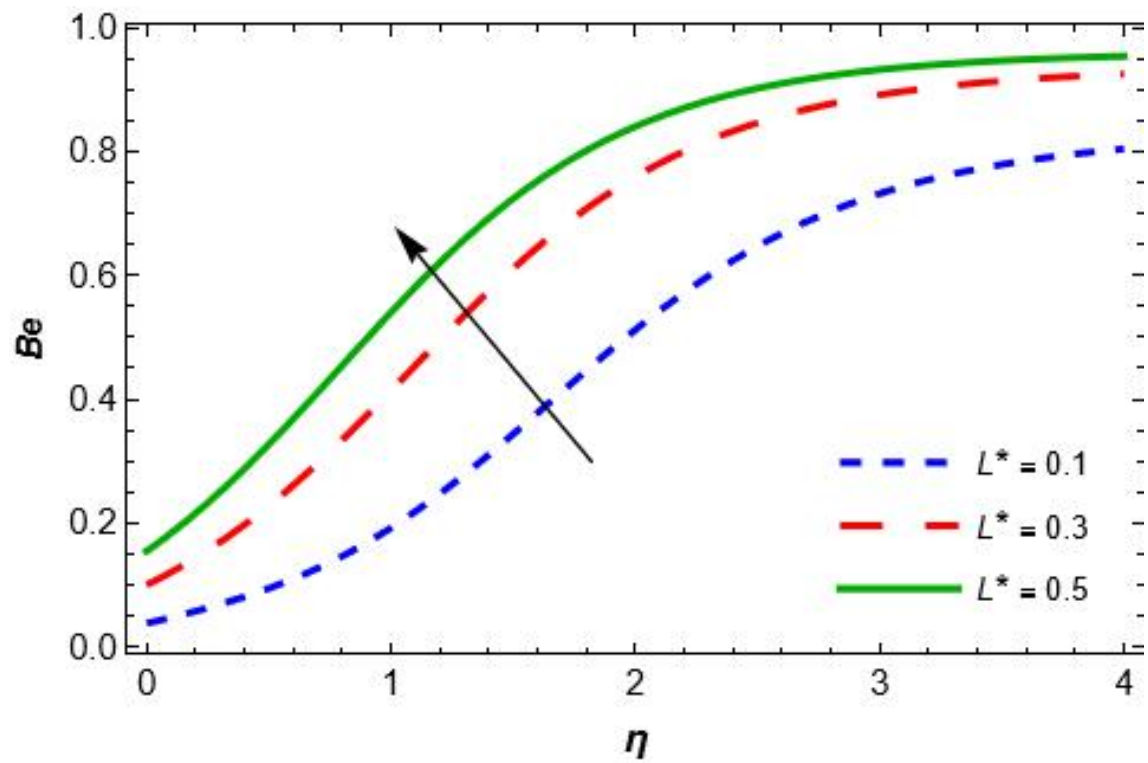
Figure 7.5:  $f'(\eta)$  for  $A$ Figure 7.6:  $f'(\eta)$  for  $f_w$

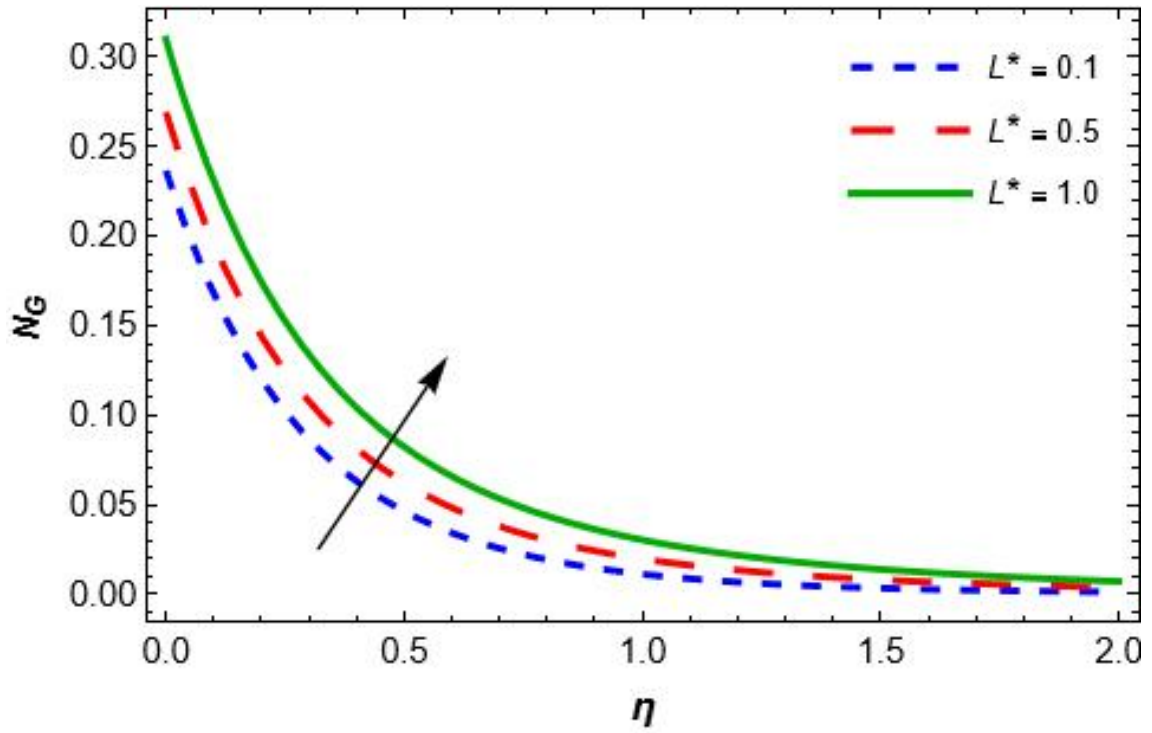
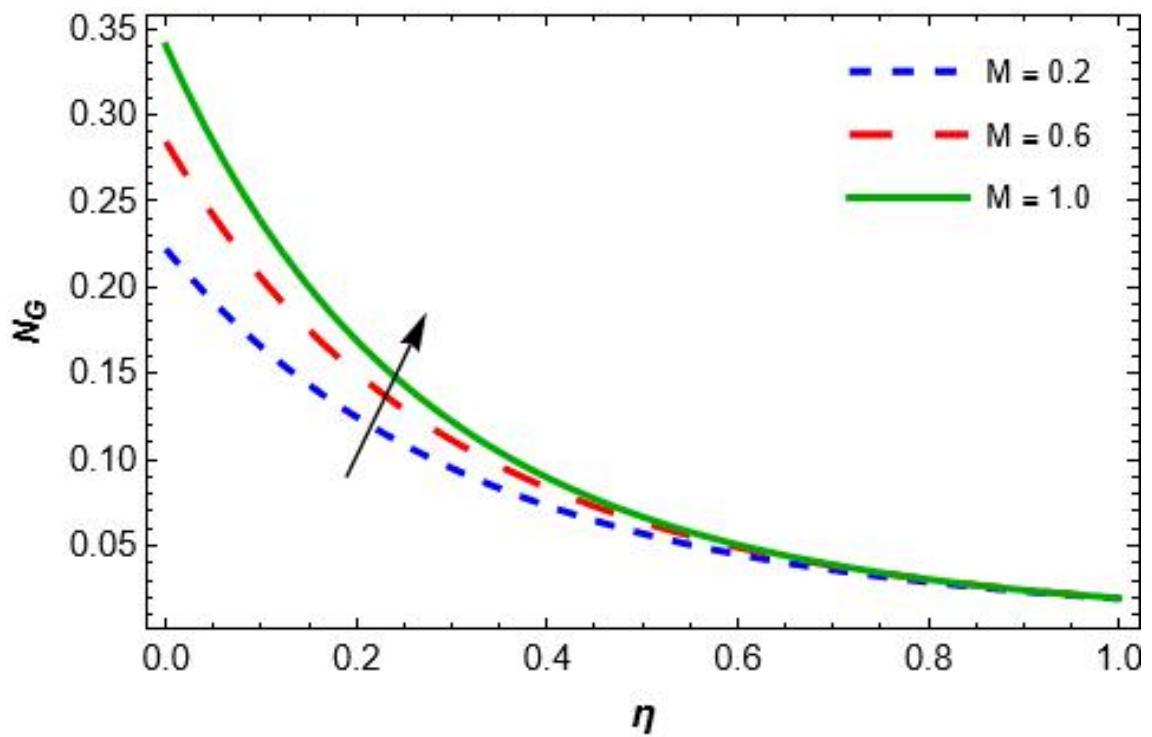
Figure 7.7:  $\theta(\eta)$  for  $M$ Figure 7.8:  $\theta(\eta)$  for  $Rd$

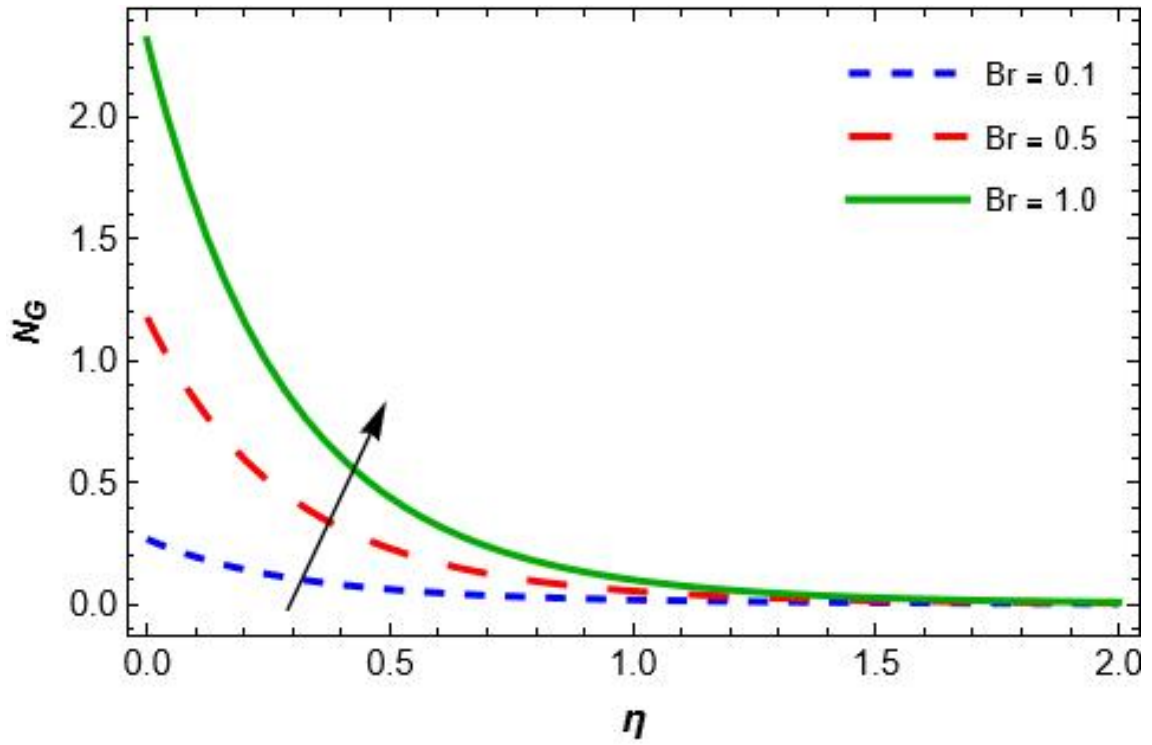
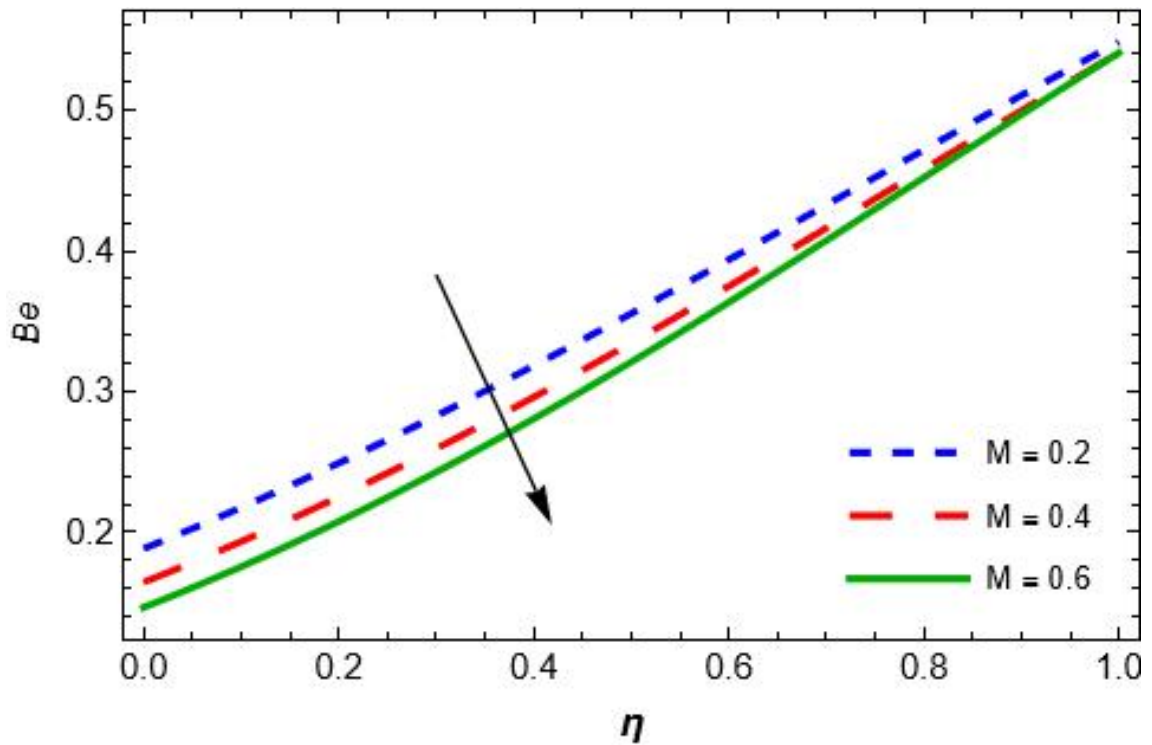
Figure 7.9:  $\theta(\eta)$  for  $\theta_w$ Figure 7.10:  $\theta(\eta)$  for  $Ec$

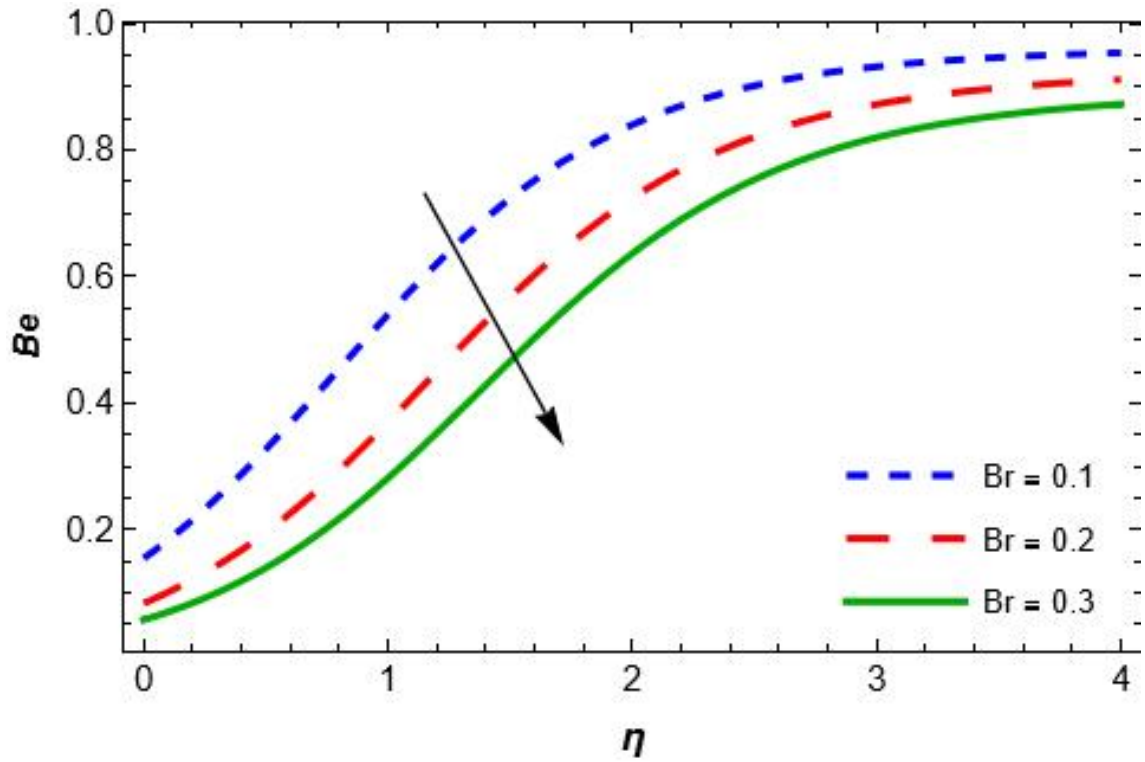
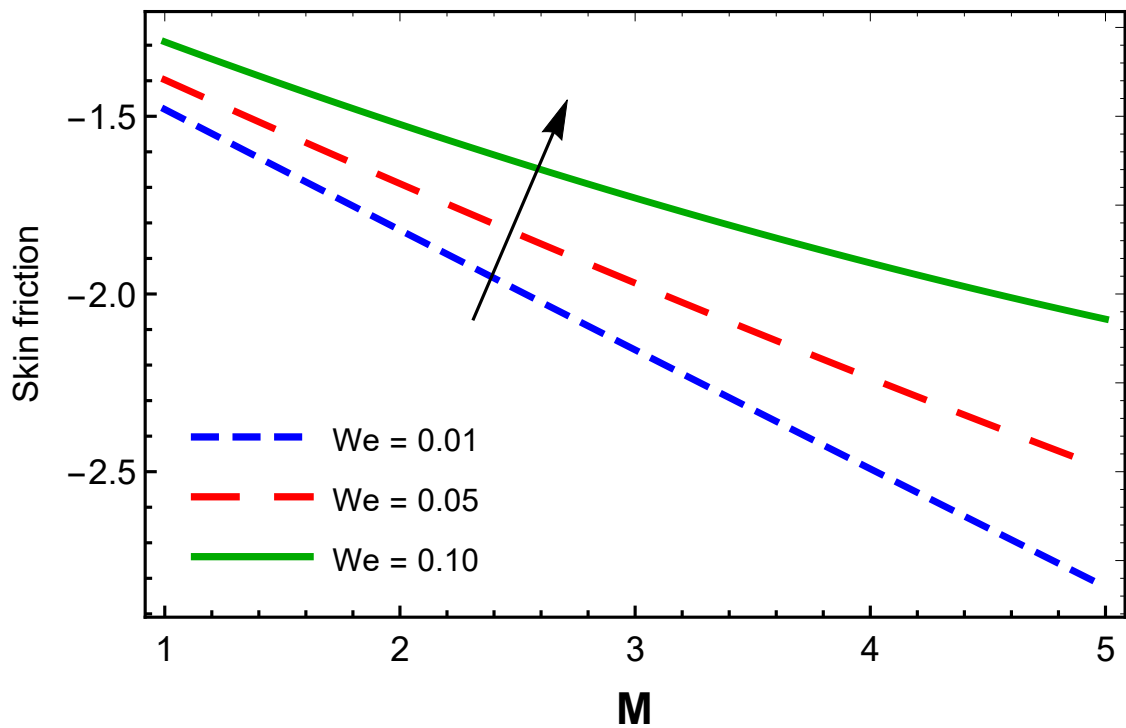
Figure 7.11:  $\theta(\eta)$  for  $Pr$ Figure 7.12:  $\theta(\eta)$  for  $A$

Figure 7.13:  $\phi(\eta)$  for  $Kc$ Figure 7.14:  $\phi(\eta)$  for  $Sc$

Figure 7.15:  $\phi(\eta)$  for  $A$ Figure 7.16:  $Be$  for  $L^*$

Figure 7.17:  $N_G$  for  $L^*$ Figure 7.18:  $N_G$  for  $M$

Figure 7.19:  $N_G$  for  $Br$ Figure 7.20:  $Be$  for  $M$

Figure 7.21:  $Be$  for  $Br$ Figure 7.22:  $C_{fx} Re_x^{1/2}$  for  $We$

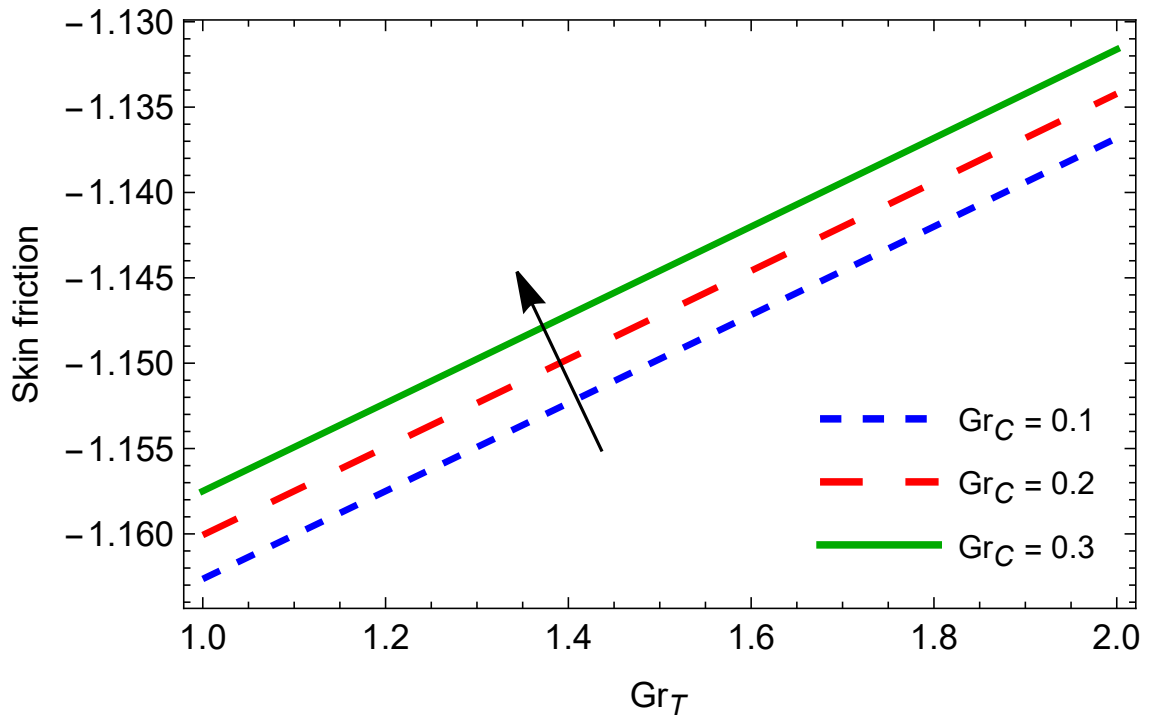
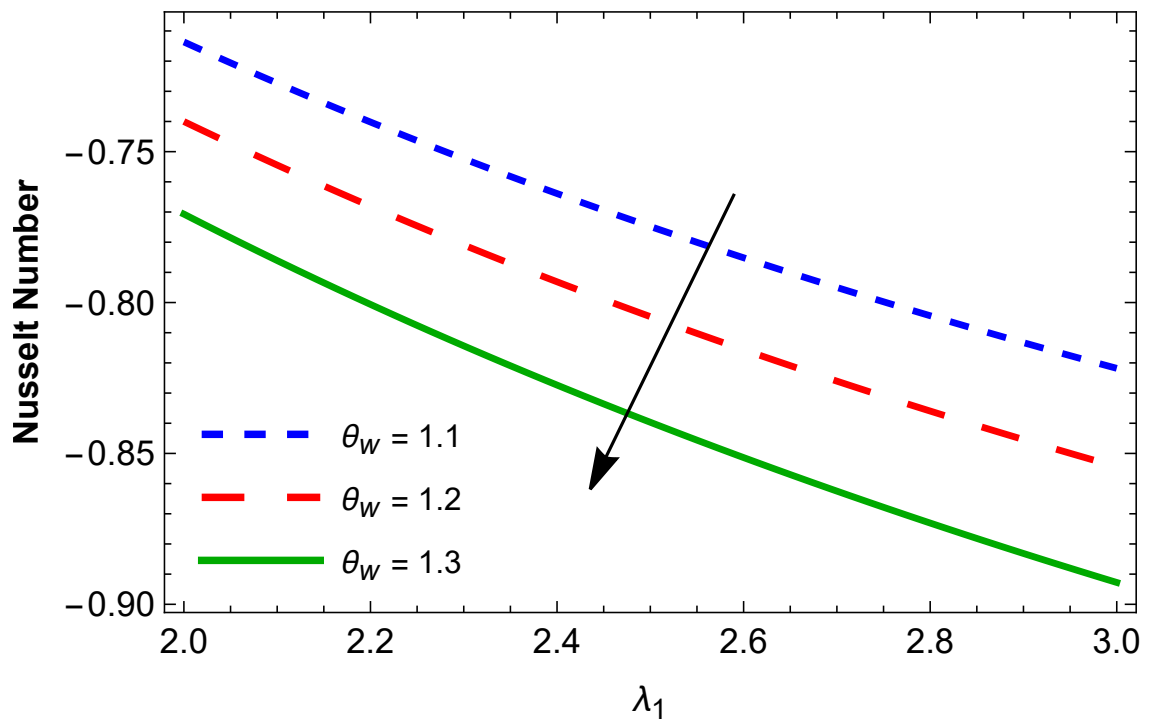
Figure 7.23:  $C_{fx} Re_x^{1/2}$  for  $Gr_C$ Figure 7.24:  $Nu_x Re_x^{-1/2}$  for  $\theta_w$

Table 7.4: Skin friction coefficient, Nusselt number and Sherwood number for the different values  $f_w, \lambda_1, \lambda_2, M, We, \gamma, Pr, Sc, A, Gr_T, Gr_C, K_c, Ec, Rd, \theta_w$ .

$f_w$	$\lambda_1$	$\lambda_2$	$M$	$We$	$\gamma$	$Pr$	$Sc$	$A$	$Gr_T$	$Gr_C$	$K_c$	$Ec$	$Rd$	$\theta_w$	$C_{fx}$	$Nu_x$	$Sh_x$
0.5	0.1	0.1	0.5	0.1	0.1	7.0	0.2	0.5	0.5	0.5	0.1	0.1	0.1	1.1	-1.1652	-0.0493	0.0871
0.6															-1.1907	-0.0448	0.0873
0.7															-1.2160	-0.0404	0.0874
	0.2														-1.1544	-0.0678	0.0871
	0.3														-1.1453	-0.0938	0.0871
		0.2													-1.1544	-0.0493	0.1541
		0.3													-1.1453	-0.0493	0.2068
			0.6												-1.1907	-0.0520	0.0871
			0.7												-1.2160	-0.0547	0.0871
				0.2											-0.9936	-0.0493	0.0871
				0.3											-0.8102	-0.0493	0.0871
					0.2										-1.0364	-0.0462	0.0870
					0.3										-0.9320	-0.0440	0.0870
						8.0									-1.1652	-0.0484	0.0871
						9.0									-1.1652	-0.0477	0.0871
							0.3								-1.1652	-0.0493	0.0895
							0.4								-1.1652	-0.0493	0.0907
								0.6							-1.1843	-0.0415	0.0874
								0.7							-1.2034	-0.0337	0.0876
									0.6						-1.1626	-0.0493	0.0871
									0.7						-1.1600	-0.0493	0.0871
										0.6					-1.1626	-0.0493	0.0871
										0.7					-1.1600	-0.0493	0.0871
											0.2				-1.1652	-0.0493	0.0873
											0.3				-1.1652	-0.0493	0.0874
												0.2			-1.1652	-0.0898	0.0871
												0.3			-1.1652	-0.1304	0.0871
													0.2		-1.1652	-0.0561	0.0871
													0.3		-1.1652	-0.0632	0.0871
														1.5	-1.1652	-0.0497	0.0871
														2.0	-1.1652	-0.0503	0.0871

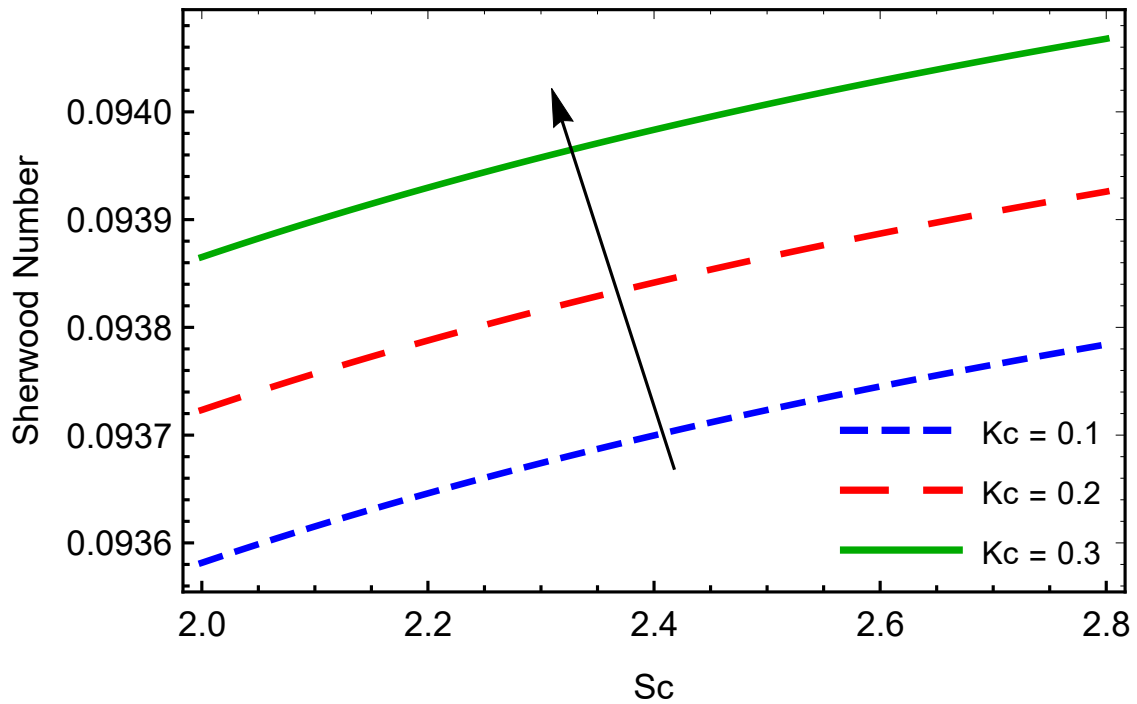


Figure 7.25:  $Sh_x Re_x^{-1/2}$  for  $Kc$

## 7.6 Conclusion

The intention of this research is to analyze joule heating, nonlinear radiation and viscous dissipation effects on entropy optimized unsteady Natural convective flow of MHD Williamson fluid across a stretching sheet with convective boundary conditions and slip condition . The main findings of the research are following:

- $M$ ,  $We$  and  $f_w$  reduces the flow.
- $M$ ,  $Rd$ ,  $\theta_w$ ,  $Ec$  improves the temperature while  $Pr$  declines temperature.
- $K_c$  and  $Sc$  increases concentration.
- $A$  reduces the flow, temperature, and concentration distribution.
- $N_G$  increases for  $L^*$ ,  $Br$  and  $M$ .
- $Be$  enhances for  $L^*$ , while declines for  $Br$  and  $M$ .
- $C_{fx}$  improves for  $Gr_C$  and  $We$ .
- $Nu_x$  declines for  $\theta_w$ , whereas  $Sh_x$  enhances for  $K_c$ .